# Triphenylamine-Based Push–Pull $\sigma$–C_60 Dyad As Photoactive Molecular Material for Single-Component Organic Solar Cells: Synthesis, Characterizations, and Photophysical Properties

Antoine Labrunie, Julien Gorenflot, Maxime Babics, Olivier Alévêque, Sylvie Dabos-Seignon, Ahmed Balawi, Zhipeng Kan, Markus Wohlfahrt, Eric Levillain, Piétrick Hudhomme, et al.

CHEMISTRY OF MATERIALS



# A triphenylamine-based push-pull – # – C60 dyad as photoactive molecular material for single-component organic solar cells: synthesis, characterizations and photophysical properties

Antoine Labrunie, Julien Gorenflot, Maxime Babics, Olivier Aleveque, Sylvie Dabos-Seignon, Ahmed H. Balawi, Zhipeng Kan, Markus Wohlfahrt, Eric Levillain, Pietrick Hudhomme, Pierre M. Beaujuge, Frédéric Laquai, Clément Cabanetos, and Philippe Blanchard

*Chem. Mater.*, **Just Accepted Manuscript** • DOI: 10.1021/acs.chemmater.8b01117 • Publication Date (Web): 23 Apr 2018

# A triphenylamine-based push-pull – σ – $C_{60}$ dyad as photoactive molecular material for single-component organic solar cells: synthesis, characterizations and photophysical properties

Antoine Labrunie,[1†] Julien Gorenflot,[2†] Maxime Babics,[2] Olivier Alévêque,[1] Sylvie Dabos-Seignon,[1] Ahmed H. Balawi,[2] Zhipeng Kan,[2] Markus Wohlfahrt,[2] Eric Levillain,[1] Piétrick Hudhomme,[1] Pierre M. Beaujuge,[2] Frédéric Laquai,[2*] Clément Cabanetos[1*] and Philippe Blanchard[1*]

[1]MOLTECH-Anjou, CNRS UMR 6200, University of Angers, 2 Bd Lavoisier, 49045 Angers, France

[2] King Abdullah University of Science and Technology (KAUST), KAUST Solar Center (KSC), Physical Sciences and Engineering Division (PSE), Material Science and Engineering Program (MSE), Thuwal 23955-6900, Kingdom of Saudi Arabia

Clement.Cabanetos@univ-angers.fr, Philippe.Blanchard@univ-angers.fr, Frederic.Laquai@kaust.edu.sa

[†] A. L. and J. G. are co-first authors of this article

## Abstract

A push-pull – σ – $C_{60}$ molecular dyad was synthesized *via* Huisgen-type click-chemistry and used as photoactive material for single-component organic solar cells. Steady-state photoluminescence (PL) experiments of the dyad in solution show a significant quenching of the emission of the push-pull moiety. Spin-casting of a solution of the dyad results in homogenous and smooth thin-films, which exhibit complete PL quenching in line with ultrafast photo-induced electron-transfer in the solid-state. Spectro-electrochemistry reveals the optical signatures of radical cations and radical anions. Evaluation of the charge carrier mobility by space-charge limited current measurements gives an electron-mobility of $\mu_e = 4.3 \times 10^{-4}$ cm$^2$ V$^{-1}$ s$^{-1}$, *ca.* 50 times higher than the hole-mobility. Single-component organic solar cells yield an open-circuit voltage $V_{oc}$ of 0.73 V and a short-circuit current density of 2.1 mA cm$^{-2}$ however, a poor fill-factor *FF* (29%) is obtained, resulting in low power conversion efficiency of only 0.4%. Combined TA and time-delayed collection field (TDCF) experiments show mostly ultrafast

photon-to-charge conversion and a small component of diffusion-limited exciton dissociation, revealing the presence of pure fullerene domains. Furthermore, a strong field dependence of charge generation is observed, governing the device fill factor, which is further reduced by a competition between extraction and fast recombination of separated charges.

## 1. Introduction

Bulk heterojunction organic solar cells (BHJ OSCs)[1-2] represent an attractive alternative to silicon technology due to their potential low-cost, flexibility, transparency and light weight. Solution-processed single-junction BHJ OSCs prepared by blending π-conjugated polymers[3-9] or molecules[10-13] as electron-donors (D), with electron-acceptors (A) such as fullerene derivatives have shown power conversion efficiencies (*PCEs*) beyond 10%[14-17,18], whereas the recent development of non-fullerene electron-acceptors[19-25] has led to record values of 13.1%.[26]

These bulk heterojunctions are created by the formation of interpenetrated networks of D and A materials, that match the typical 5-10 nm exciton diffusion length of organic semiconductors[4, 27] and exhibit: i) an increased interfacial contact area between domains of D and A, providing more exciton dissociation sites, and ii) a continuous pathway enabling the transport of both holes and electrons to the electrodes. Thus, after light absorption, the excitons generated in D and/or A domains can diffuse to the D/A interface where an energy offset between the donor and acceptor molecular orbitals facilitates their dissociation into spatially-separated holes and electrons that can drift-diffuse to the electrodes hence generating a photocurrent.[27-29]

However, the fabrication of efficient BHJ OSCs requires careful optimization of the morphology of the photoactive layer by empiric optimization of the D/A concentrations and ratio, the nature of the solvent and co-solvent (use of additives) as well as the film-processing conditions (thermal and/or solvent vapor annealing).[30-31] Importantly, the 'optimum' morphology of the photoactive layer may not be thermodynamically stable and typically evolves by spontaneous component demixing, especially when fullerene derivatives are used, leading to detrimental effects on the PV performance.[2]

To tackle some of the difficulties associated with BHJ OSCs, so-called "*Molecular Heterojunction*"[32] and "*Double-cable polymer*"[33] approaches were proposed a few years ago. These strategies rely on the use of a single photo-active material where the donor and the acceptor components are covalently linked through a non-conjugated σ-connector.[34-38] Besides, their interesting photophysical[39-42] and self-assembly[43] properties, these types of materials were explored for the fabrication of single-component organic solar cells (SC-OSCs). It was expected that the morphology of such photoactive layer would be less subjected to morphology evolution and that the relative close proximity of the D and A blocks would favor exciton dissociation on

the same molecule, thereby avoiding the limiting step of exciton diffusion associated with organic semiconductors.

Despite the fundamental interest in this concept, most materials evaluated in SC-OSCs led to *PCE* values often much below 0.5%.[34, 36-37, 42, 44-48] These poor PV performances could be assigned to high fractions of geminate charge recombination within the bi-functional material and to the difficulty to form an efficient charge carrier percolation network for the extraction of charges at the electrodes.[40, 42, 46, 48]

However, renewed interest in this concept has been triggered by recent publications demonstrating control of self-assembly and microphase separation in block copolymers.[49-50] For instance, fullerene-grafted polythiophene-based co-polymers[51,52] or diketopyrrolopyrrole-based conjugated polymers with perylene bisimide side chains[53] have recently led to efficient polymer based SC-OSCs with *PCEs* up to 5%. Self-assembly of liquid-crystalline extended monodisperse donor-acceptor block co-oligomers based on fluorene-bithiophene and perylene bisimide were also investigated and showed long-range ordered domains[54-57] leading to SC-OSCs with *PCEs* ranging between 1.50-2.30%.[54-55]

On the other hand, following the seminal work of Nierengarten *et al.*,[32, 47] few discrete molecular assemblies, essentially fullerene-based π-conjugated systems,[34-38, 44-47] have been investigated for SC-OSCs. Compared to polymers, these small molecules exhibit several advantages such as a well-defined structure, allowing more precise understanding of structure-property relationships, an easier purification, and a better reproducibility in terms of synthesis.[58] To the best of our knowledge, the best PV performance of related SC-OSCs has been recently obtained with very few dyads or triads incorporating fullerene derivatives as acceptor units linked to electron-rich π-conjugated systems based on oligo(*p*-phenylenevinylene) (*PCE* = 1.28% with $C_{60}$ and 1.92% with $C_{70}$),[59-60] thiophene-diketopyrrolopyrrole (*PCE* = 0.53-1.11%)[61-62] and dithienosilole-dibenzothiadiazole (*PCE* = 0.4%).[63] Since 2016, a dithiafulvalene-functionalized diketopyrrolopyrrole-$C_{60}$ dyad and a triad based on an oligothiophene-fullerene conjugate were reported with promising and encouraging *PCEs* of 2.2% and 2.4%.[64-65]

Although the development of SC-OSCs remains very challenging, these last results on small molecules suggest that enhanced PV performance can be obtained by proper design of new D and A components, by playing with the nature of the spacer between D and A, and/or by controlling the self-assembly of resulting discrete molecular assemblies.

Recently, we reported the use of a small and easily accessible push-pull molecule **TPA-T-DCV** (Scheme 1) as active electron-donor for OPV. For instance, bilayer planar heterojunction or hybrid co-evaporated BHJ OSCs combining **TPA-T-DCV** with $C_{60}$ as electron acceptor material led to *PCEs* of 2.5%[66] and 4.0%[67], respectively, while solution-processed BHJ OSCs blended with $PC_{61}BM$ gave *PCEs* of 3.0%.[68] The PV performance of this key molecule was further optimized through subtle structural modifications.[66, 68-69, 70, 71-72]

Herein, the structure of the push-pull **TPA-T-DCV** molecule has been altered for subsequent functionalization by one $C_{60}$ unit affording the targeted compound **TPA-T-$C_{60}$** (Scheme 1). The synthesis of this push-pull – σ – $C_{60}$ dyad is described together with its electrochemical and optical properties. The PV performance of **TPA-T-$C_{60}$** has been evaluated in simple SC-OSCs. Exciton dissociation and charge generation were studied on thin-films of **TPA-T-$C_{60}$** and on the methyl-cyanoacrylate reference push-pull compound **TPA-T-MCA** without fullerene unit. Finally, the photo-induced processes occurring in SC-OSCs have been analyzed by transient absorption spectroscopy combined with time delayed collection field experiments to evaluate the mechanisms of charge generation and recombination.

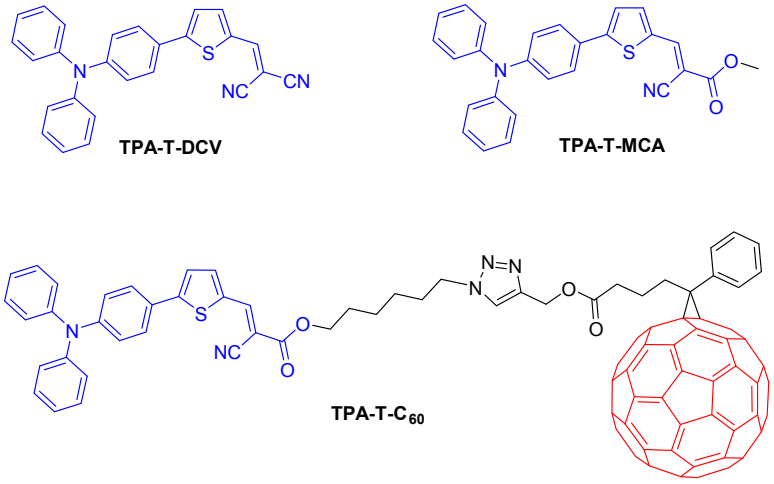


**Scheme 1.** Structures of **TPA-T-DCV** and **TPA-T-MCA** push-pull molecules and **TPA-T-$C_{60}$** dyad

## 2. Results and discussion

**2.1. Synthesis of TPA-T-$C_{60}$.** Our synthetic strategy is based on the replacement of one of the two nitrile groups of **TPA-T-DCV** by an ester group allowing for the subsequent functionalization with a modified $C_{60}$ unit *via* click-chemistry (Scheme 2). A Knœvenagel

condensation between the previously described aldehyde **TPA-T-CHO**[66, 73-74] and the hitherto unreported $CH_2$-activated compound **1**, namely 6-azidohexyl 2-cyanoacetate, led to the azido-functionalized push-pull molecule **TPA-T-N$_3$** in 91% yield. The latter was engaged in a copper(I)-catalyzed 1,3-dipolar Huisgen cycloaddition with the [*6,6*]-phenyl-$C_{61}$ butyric acid propargyl ester **2** under strict anaerobic conditions leading to the selective formation of a 1,2,3-triazole ring and hence affording the target dyad **TPA-T-C$_{60}$** in 80% yield. Compound **TPA-T-MCA** was prepared by Knœvenagel condensation between **TPA-T-CHO** and methyl 2-cyanoacetate (see SI).

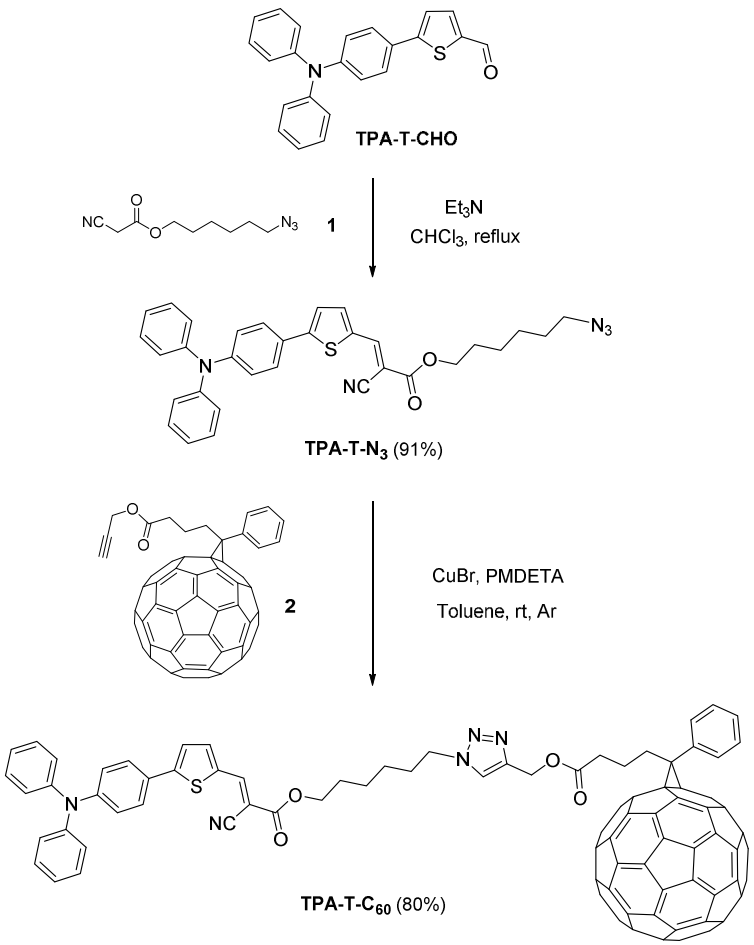


**Scheme 2**. Synthetic route to **TPA-T-C$_{60}$**

The synthesis of the new σ-spacer block **1** and that of propargyl ester **2** using a slightly modified procedure are described in Supporting Information.[75,76,77]

After a straightforward purification by column chromatography, the thermal stability of the dyad has been assessed by thermogravimetric analysis (Figure S10), showing a decomposition temperature ($T_d$) value of 284 °C defined at 5% weight loss.

**2.2. Electrochemical and Optical Properties.** The electrochemical properties of **TPA-T-C$_{60}$** were investigated by cyclic voltammetry in $CH_2Cl_2$ in the presence of $Bu_4NPF_6$ as supporting electrolyte under a controlled argon atmosphere and compared to those of the **TPA-T-N$_3$** and **PC$_{61}$BM**. The cyclic voltammogram (CV) of **TPA-T-C$_{60}$** has been recorded between – 1.8 V and + 0.8 V *vs* $Fc/Fc^+$ (Figure 1). It first shows a reversible one-electron oxidation wave peaking at $E_{pa}$ = + 0.57 V *vs* $Fc/Fc^+$ that can be assigned to the formation of the stable radical cation of the push-pull donor moiety of the dyad in agreement with the CV of **TPA-T-N$_3$**. Furthermore, two successive reversible reduction waves are observed at $E_{pc}$ of – 1.15 V and – 1.53 V *vs* $Fc/Fc^+$ attributed to the step-by-step one-electron reduction of the fullerene moiety as deduced from the electrochemical signature of **PC$_{61}$BM** recorded under the same conditions. The third irreversible reduction process at $E_{pc}$ = – 1.69 V *vs* $Fc/Fc^+$ for **TPA-T-C$_{60}$** is attributed to the formation of the radical-anion of the push-pull system, once again in agreement with the CV of **TPA-T-N$_3$**.

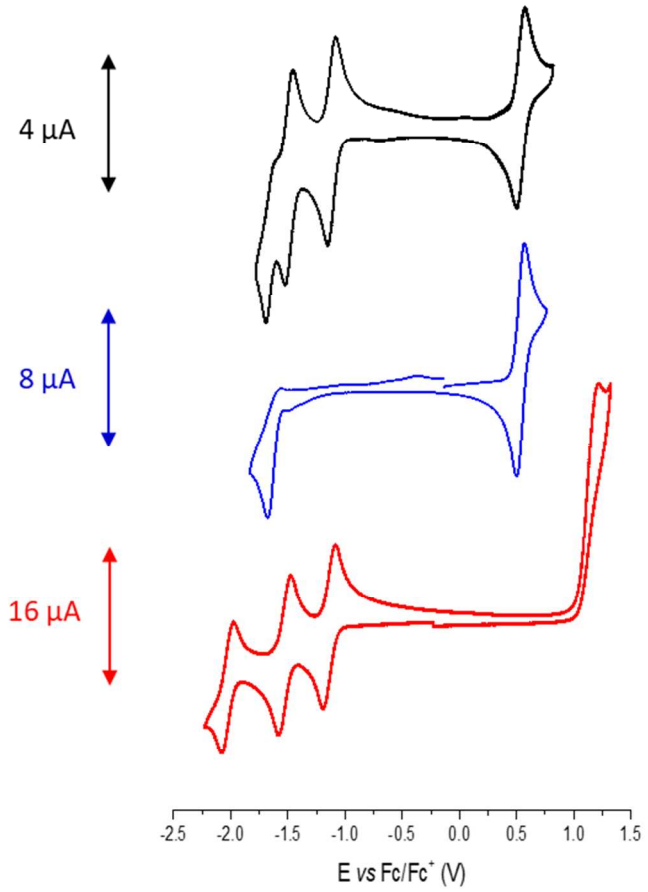


**Figure 1.** Cyclic voltammograms of **TPA-T-C$_{60}$** (black, 0.5 mM), **TPA-T-N$_3$** (blue, 1 mM) and **PC$_{61}$BM** (red, *ca.*1 mM) in 0.1 M $Bu_4NPF_6/CH_2Cl_2$, scan rate 100 mV $s^{-1}$, Pt working and counter electrodes.

**Table 1.** Cyclic voltammetric data of **TPA-T-C$_{60}$** and building-block intermediates (in 0.1 M $Bu_4NPF_6/CH_2Cl_2$, scan rate 100 mV $s^{-1}$, Pt working and counter electrodes).[a]

| Compd | $E_{pc}$ (V) | | | | $E_{pa}$ (V) | |
|---|---|---|---|---|---|---|
| **TPA-T-C$_{60}$**[b] | --- | - 1.69 irr. | - 1.53 | - 1.15 | + 0.57 | --- |
| **TPA-T-N$_3$**[b] | --- | - 1.69 irr. | --- | --- | + 0.57 | --- |
| **PC$_{61}$BM** | - 2.08 | --- | - 1.58 | - 1.19 | --- | + 1.21 |

[a] Potentials are expressed *vs.* ferrocene/ferrocenium redox couple recorded in the same conditions. [b] Oxidation and reduction peaks were recorded between – 1.8 V and + 0.8 V.

The optical properties of the dyad **TPA-T-C$_{60}$**, the push-pull azido precursor **TPA-T-N$_3$** and **PC$_{61}$BM** have been then analyzed in diluted $CH_2Cl_2$ solutions by UV-vis absorption (*ca.* $10^{-5}$ M) and photoluminescence emission (*ca.* $10^{-6}$ M) spectroscopy (Table 2).

The UV-vis spectrum of **TPA-T-N$_3$** shows two main absorption bands, the first one at high energy with a maximum ($\lambda_{max}$) at 303 nm and a second broad and intense one centered at 476 nm assigned to an internal charge transfer (ICT) from the TPA moiety to the electron-withdrawing cyanoacrylate group (Figure 2).

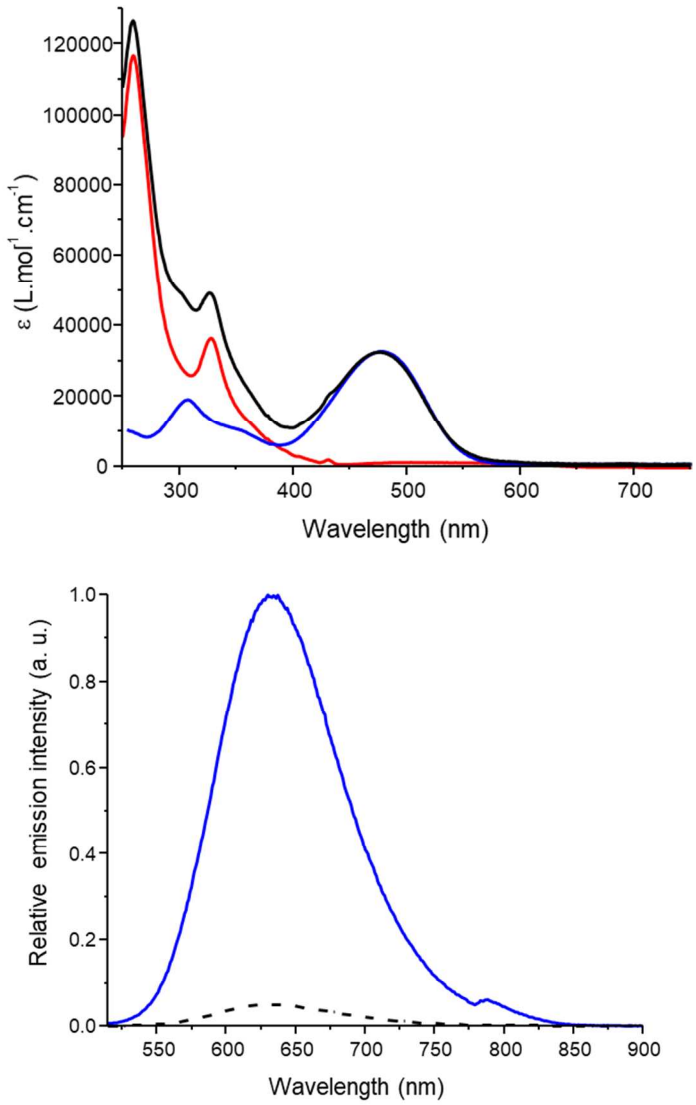


**Figure 2.** Top: UV-vis absorption spectra of **TPA-T-C$_{60}$** (black line), **TPA-T-N$_3$** (blue line) and **PC$_{61}$BM** (red line) recorded at 20 °C in $CH_2Cl_2$. Bottom: relative emission spectra of **TPA-T-N$_3$** (blue line) and **TPA-T-C$_{60}$** (black dashed line) recorded at 20 °C in $CH_2Cl_2$ solutions exhibiting the same optical density at $\lambda_{exc}$ = 500 nm.

The target dyad **TPA-T-C$_{60}$** exhibits a broad absorption band at 478 nm characteristic of the push-pull moiety. The grafting of the fullerene unit by click-chemistry is confirmed by the presence of specific absorption bands at $\lambda_{max}$ = 259 nm and 327 nm, and a discernable band at

431 nm in accordance with the UV-vis spectrum of **$PC_{61}BM$** (Figure 2). To summarize, the UV-vis spectrum of the target dyad **TPA-T-$C_{60}$** corresponds to the superimposition of the optical signature of **TPA-T-$N_3$** with that of **$PC_{61}BM$** suggesting the absence of electronic coupling in the ground state between the push-pull chromophore and the fullerene moiety.

**Table 2.** UV-vis absorption and emission data in $CH_2Cl_2$.[a]

| Compd | $\lambda^{abs}_{max}$/nm ($\varepsilon$/$M^{-1}$ $cm^{-1}$) | $\lambda^{em}_{max}$/nm | $\Phi_f$/% |
|---|---|---|---|
| **TPA-T-MCA** | 303 (20300), 477 (35000) | 632 | 16 |
| **TPA-T-$N_3$** | 303 (20100), 476 (34000) | 630 | 18 |
| **TPA-T-$C_{60}$** | 259 (126000), 300 (*sh*, 47300), 327 (48500), 431 (*sh*, 19600), 478 (32400), 692 (400) | 630 | 1 |
| **$PC_{61}BM$** | 259 (117400), 328 (36800), 431 (2800), 492 (1700), 687 (400) | *n. d.*[b] | *n. d.*[b] |

[a] Rhodamine B ($\Phi_f$ = 0.50% in EtOH) was used as standard for fluorescence quantum yield measurements.[78] The excitation wavelength was set at 500 nm. [b] Not determined.

The photoexcitation of **TPA-T-$N_3$** at $\lambda_{exc}$ = 500 nm leads to photoluminescence with an emission maximum at 630 nm associated to a fluorescence quantum yield of 18% (Table 2). Interestingly, the dyad **TPA-T-$C_{60}$** shows also photoluminescence properties with the same emission maximum as the azido precursor however, the fluorescence quantum yield decreases significantly to 1% suggesting the occurrence of either a photo-induced electron transfer or an energy transfer in solution from the photo-excited electron-donor push-pull chromophore to the electron-accepting fullerene unit (Figure 2). The origin of this quenching of fluorescence in solution will be discussed further below; here this preliminary result underlines the potential of the target dyad as active material for single-component OSCs.

It is worth mentioning also that both **TPA-T-$N_3$** and **TPA-T-$C_{60}$** exhibit a noticeable Stokes shift. This behavior is solely related to the push-push moiety in agreement with the optical properties of the reference compound **TPA-T-MCA** ($\lambda^{abs}_{max}$ = 477 nm and $\lambda^{em}_{max}$ = 632 nm). In

fact, this noticeable Stokes shift has already been observed in other push-pull molecules[79-80] and is associated to an efficient intramolecular charge transfer[69] probably leading to geometrical changes between the ground and excited states, further theoretical work would be necessary to confirm this last hypothesis.

**2.3. Spectroelectrochemistry.** In parallel, the dyad **TPA-T-C$_{60}$** has also been analyzed in solution by spectroelectrochemistry in order to gain information on the optical signature of the corresponding radical cation push-pull$^{+\bullet}$ – σ – $C_{60}$ and radical anion push-pull – σ – $C_{60}^{-\bullet}$ states (Figure 3). Cyclic voltammetry in thin layer conditions (50 µm) of a millimolar solution of **TPA-T-C$_{60}$** in 0.1 M $Bu_4NPF_6/CH_2Cl_2$ was performed in oxidation and reduction conditions, according to the current *vs* time profile reported in Figure 3 and the corresponding variation of absorbance was simultaneously recorded in the UV-vis-NIR region.

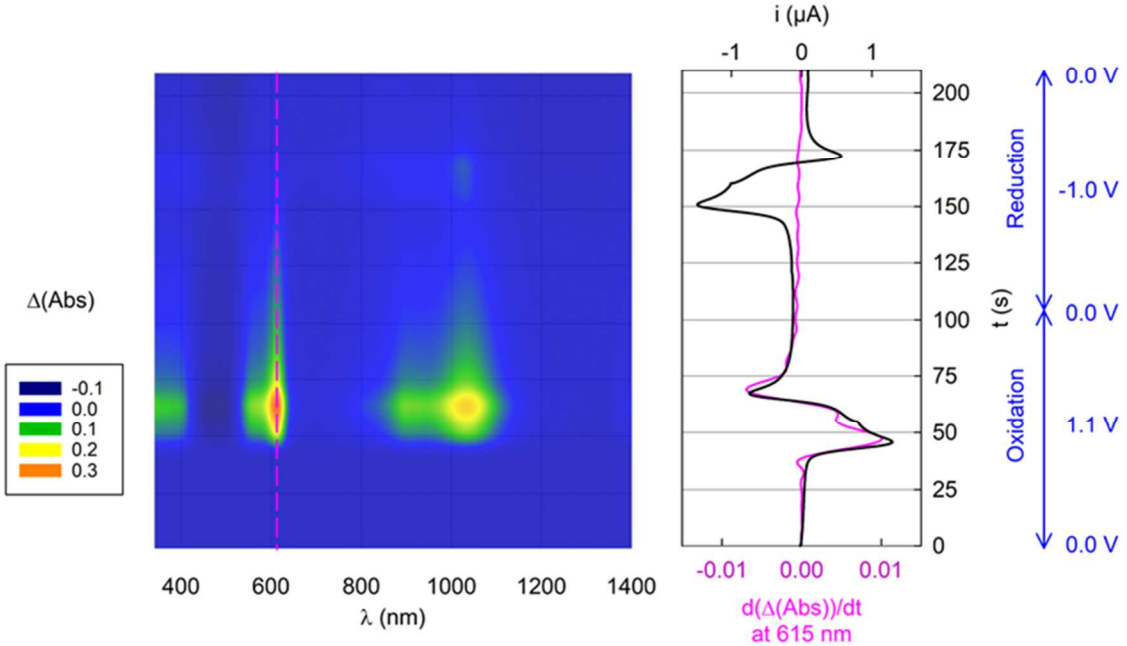


**Figure 3.** Absorption spectroelectrochemistry experiment in thin layer conditions (50 µm) during a cyclic voltammetry experiment (over oxidation and reduction) of a solution of 1 mM of **TPA-T-C$_{60}$** in 0.1 M $Bu_4NPF_6/CH_2Cl_2$ at 20 mV/s and 20 °C. Left: 3D representation: *x* axis = wavelength (nm), *y* axis = time (s), and *z* axis = variation of absorbance. Right: Comparison between time *vs*. current and time *vs*. d(absorbance)/dt at 615 nm. *Note that the variation of absorbance at a given potential was determined by comparison with a reference spectrum recorded at the equilibrium potential.*

Upon oxidation of **TPA-T-C$_{60}$**, (40 s < time < 80 s), the absorption band characteristic of the neutral push-pull moiety at 478 nm decreased. In parallel, a relatively weak absorption band between 345 and 400 nm appeared together with two strong broad absorption bands peaking at 610 and 1033 nm exhibiting shoulders at 559 and 913 nm, respectively. These optical signatures are attributed to the cation radical push-pull$^{+\bullet}$ – σ – $C_{60}$. Electrochemical reduction of **TPA-T-C$_{60}$** to the radical anion push-pull – σ – $C_{60}^{-\bullet}$ (150 s < time < 180 s) is essentially accompanied by the appearance of a weakly discernable band centered at 1030 nm. This latter result is entirely consistent with the reported absorption maximum at 1040 nm for the radical-anion of methanofullerene derivatives generated upon radiation-induced reduction in organic solvents[81] as well as with the electronic transition at 1.2 eV (*ca*. 1033 nm) for $PC_{61}BM^{-\bullet}$ obtained from photo-induced absorption measurements on a mixture of an oligo(*p*-phenylene vinylene) and $PC_{61}BM$ or an oligo(*p*-phenylene ethynylene vinylene) covalently linked to $C_{60}$.[82] The optical signatures of the electrogenerated cation radical and radical anion of the dyad molecule are useful for comparison with those of the corresponding photogenerated species (*vide infra*). However, clearly the weak absorption band at 1030 nm specific to the radical anion push-pull – σ – $C_{60}^{-\bullet}$ is extremely difficult to detect by transient absorption spectroscopy, because of the concomitant formation of the cation radical push-pull$^{+\bullet}$ – σ – $C_{60}$ which is expected to show a stronger absorption in the same NIR region (see below).

**2.4. Thin Films Morphology, Charge Transport Properties and Single-Component Photovoltaic Performance.** Homogeneous thin-films on glass were readily prepared by spin-coating of a $CHCl_3$ solution of **TPA-T-C$_{60}$**. Compared to the solution, the absorption spectrum of the thin-films shows a slight bathochromic shift of the ICT band (+8 nm) and the bands associated to the fullerene moiety (*ca*. +5 nm) (Figure S11). Owing to the good film-forming properties of **TPA-T-C$_{60}$**, hole ($\mu_h$) and electron ($\mu_e$) mobilities were estimated by the space-charge-limited current (SCLC) method using hole-only and electron-only devices of architectures ITO/PEDOT-PSS (40 nm)/**TPA-T-C$_{60}$** (110 nm)/Au (150 nm) and ITO/**TPA-T-C$_{60}$** (110 nm)/LiF (1 nm)/Al (100 nm) respectively (Figure S12). Hence, a $\mu_h$ value of *ca* $7.8 \times 10^{-6}$ cm$^2$ V$^{-1}$ s$^{-1}$ and a $\mu_e$ value of *ca* $4.3 \times 10^{-4}$ cm$^2$ V$^{-1}$ s$^{-1}$ were measured. These results highlight the ambipolar semiconducting behaviour of **TPA-T-C$_{60}$**, albeit with a $\mu_e/\mu_h$ ratio of *ca*. 50 evidencing better electron-transporting properties.

The photovoltaic properties of **TPA-T-C$_{60}$** have been evaluated in single-component organic solar cells (SC-OSCs) of 0.10 cm$^2$ area with the following basic configuration: ITO (109 nm)/PEDOT:PSS (*ca.* 26 nm)/**TPA-T-C$_{60}$** (*ca*. 50 nm)/Ca (6 nm)/Al (100 nm). Best efficiencies were obtained with an active layer deposited by spin-coating from a solution of **TPA-T-C$_{60}$** in $CHCl_3$ (15 mg/mL) at 4000 rpm.

Figure 4 shows the best current density-voltage *J-V* characteristic measured under AM 1.5 simulated solar illumination (100 mW cm$^{-2}$). Single-component devices fabricated from **TPA-T-C$_{60}$** show photovoltaic conversion with a *PCE* of 0.4% associated to an open-circuit voltage $V_{oc}$ of 0.73 V, a short-circuit current density $J_{sc}$ of 2.1 mA cm$^{-2}$ and a low fill-factor *FF* of 29%.

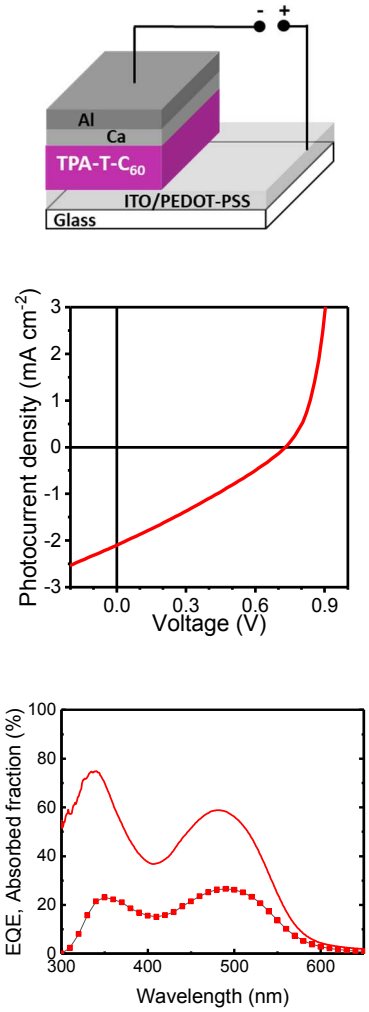


**Figure 4.** Top: structure of the device. Middle: *J–V* characteristics of the best SC-OSC based on **TPA-T-C$_{60}$** in under AM 1.5 simulated solar light under illumination. Bottom: corresponding EQE (symbols) and absorption efficiency (continuous line) of the **TPA-T-C$_{60}$** active layer in a device structure ITO (109 nm)/PEDOT:PSS (*ca*. 26 nm)/**TPA-T-C$_{60}$** (*ca*. 50 nm)/Ca (6 nm)/Al (100 nm) as calculated using transfer matrix formalism (*vide infra*) This gives an internal quantum efficiency comprised between 30 and 50%.

The external quantum efficiency (*EQE*) spectrum of the champion SC-OSCs, performed under monochromatic irradiation, extends from 310 to 650 nm (Figure 4). The two bands peaking at 360 nm and *ca*. 500 nm, are attributed to the contribution of the fullerene and the push-pull moieties of **TPA-T-C$_{60}$** respectively, in agreement with the absorption spectrum of the simulated absorption of the active layer. The integration of the surface area of the *EQE* spectrum gives a current-density value *J* of *ca*. 2.06 mA cm$^{-2}$ which is in close agreement with the $J_{sc}$ (2.1 mA cm$^{-2}$) value obtained from the *J vs. V* curve measured on SC-OSCs under white light illumination.

In order to gain more information on the morphology of the active layer, its nanoscale topography was analyzed by atomic force microscopy (AFM) and transmission electron microscopy (TEM). The AFM images show that the surface of the active layer is very smooth with a root-mean-square (RMS) roughness of *ca* 0.7 nm. While TEM images essentially show homogenous films, suggesting the lack of phase-segregated domains with size higher than 10 nm (Figure 5), the occurrence of darker domains confirmed also the existence of PC$_{61}$BM-rich regions.

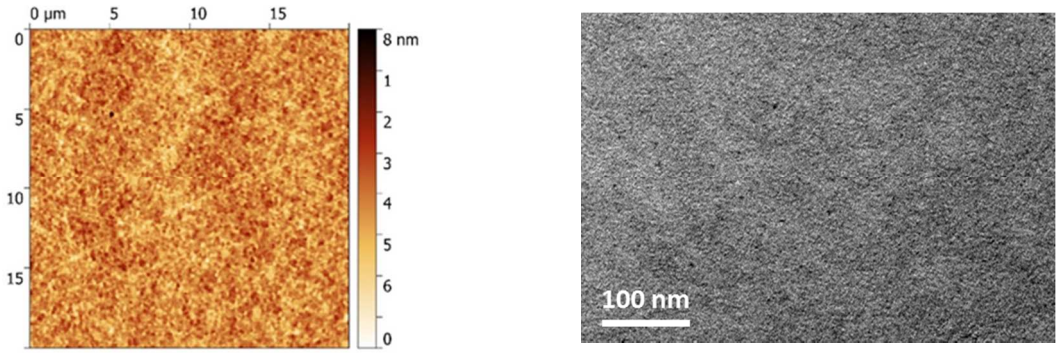


**Figure 5.** AFM (left) and TEM (right) images of a thin-film of **TPA-T-C$_{60}$**.

**2.5. Photophysical Experiments.** Understanding OPV performance, specifically the efficiency-limiting processes in **TPA-T-C$_{60}$**-based solar cells, requires insight into the elementary steps determining photocurrent generation efficiency: 1.) photon absorption leading to exciton formation, 2.) charge transfer, either ultrafast or following exciton diffusion towards the donor:acceptor heterojunction, 3.) charge separation competing with geminate recombination of interfacial charge transfer states on a nanosecond timescale, and finally 4.) nongeminate recombination of separated charges, competing with extraction on a nanosecond to hundreds of microseconds timescale. Transient absorption spectroscopy (TA) is one of the few techniques

able to monitor all excited states across the sub-picoseconds to hundreds of microseconds time range and was applied here. Here, we combined the TA with data from a transient charge extraction technique, namely time-delayed collection field (TDCF), to quantify the densities of charges present in the bulk heterojunction as very recently described by us for other OPV systems.[83]

**2.5.1. Absorption and photocurrent.** The full wavelength dependent absorption, reflection, and interference pattern within the device stack was obtained *via* transfer matrix optical simulations[84] using the refractive index of the individual layers independently obtained by ellipsometry (see supporting information, SI). Only the fraction of light absorbed in the photoactive layer of the ITO (109 nm)/PEDOT:PSS (25 nm)/**TPA-T-C$_{60}$** /Ca (6 nm)/Al (100 nm) solar cell can be converted into photocurrent. Figure 6 shows the predicted maximal photocurrent as function as the photoactive layer thickness, for a quantitative conversion of absorbed photons into free charges and their extraction. As can be seen, while the experimental values of $J_{sc}$ match the curve for the thinnest samples, a deviation occurs when the thickness $d$ increases. This could be due to less efficient charge separation (due to the decrease of the electric field, close to $V_{OC}/d$ in short circuit conditions, assisting charge separation) and/or due to charge extraction competing with recombination (as the extraction time increases with the distance to the electrodes, thus with the thickness). This prevents us from using thicker samples, which would ensure maximum light collection. The loss with increasing thickness is an important bottleneck to be addressed in future work.

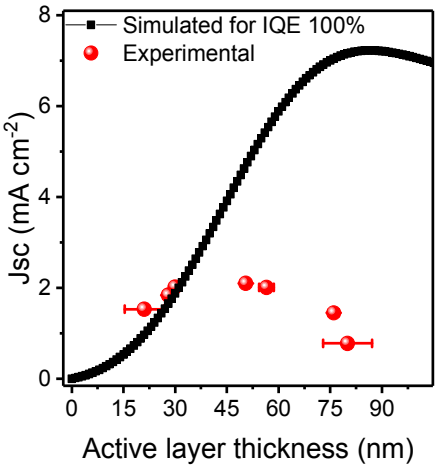

**Figure 6.** Experimentally observed and theoretically predicted photocurrent as a function of the photoactive layer thickness of a ITO/PEDOT:PSS/**TPA-T-C$_{60}$**/Ca/Al device (with thicknesses of 109/25/x/100 nm). The transfer matrix code used for these simulations was developed by George F. Burkhard and Eric T. Hoke. The code is freely available from: http://web.stanford.edu/group/mcgehee/transfermatrix/index.html and was adapted from the procedures originally described in Ref. [27] and [84].

**2.5.2. Exciton dissociation and charge generation.** Transient absorption spectroscopy across the time range from sub-picoseconds to several nanoseconds reveals the mechanisms of charge generation in **TPA-T-C$_{60}$**. As we will demonstrate below, four main observations are made from this experiment: 1) a weak or negligible electronic coupling between the push-pull donor and the PC$_{61}$BM-derived acceptor moieties of the dyad in solution, 2) the formation of PC$_{61}$BM-derived triplet states in **TPA-T-C$_{60}$** solutions accompanying singlet exciton decay, 3) an ultrafast generation of charges in **TPA-T-C$_{60}$** films and finally, 4) an additional exciton diffusion-limited charge generation from fullerene–rich domains in **TPA-T-C$_{60}$** films.

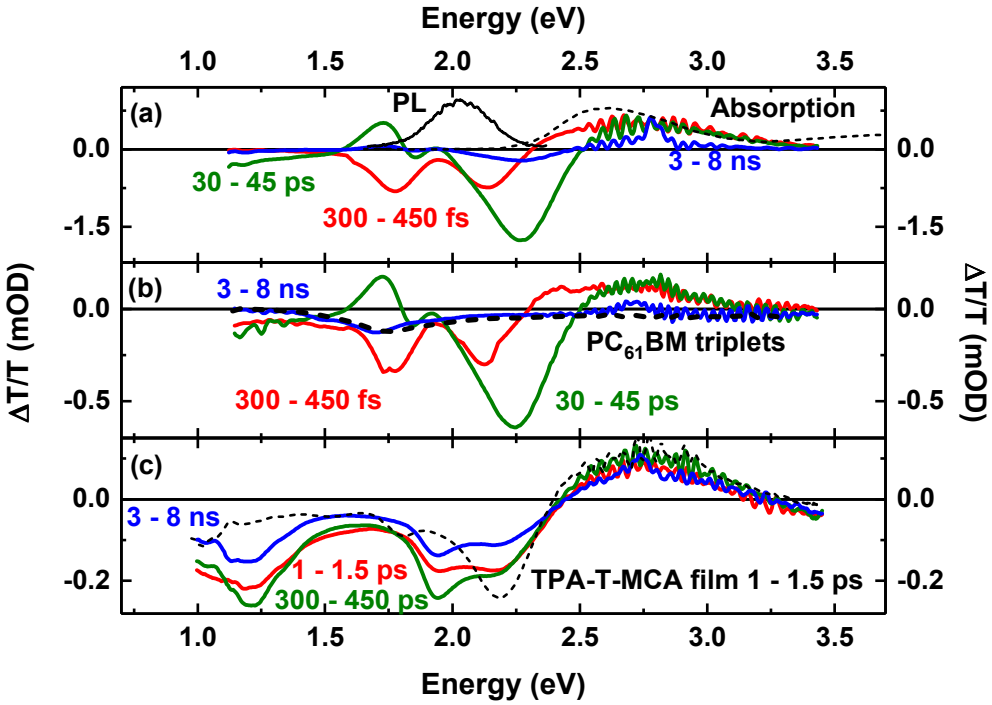


**Figure 7.** Transient absorption spectra of: (a) **TPA-T-MCA** building block 0.1 mM in chloroform solution (excitation at 475 nm, 11 $\mu$ J/cm$^2$ per pulse) together with the transient photoluminescence (t-PL, integrated from 0 to 8 ns), and UV-Vis absorption spectrum of the same solution for comparison, (b) the dyad **TPA-T-C$_{60}$** 0.1 mM in chloroform (excitation at 480 nm, 3.3 μJ/cm$^2$ per pulse) together with the spectral signature from triplets of **PC$_{61}$BM** measured from a 0.1 mM chlorobenzene solution, and (c) a **TPA-T-C$_{60}$** thin film (excitation at 480 nm, 3 $\mu$ J/cm$^2$ per pulse) and exciton-induced absorption spectrum of the building block **TPA-T-MCA** in thin film for comparison.

The TA spectra of solutions (Figure 7a and 7b) indicate weak electronic coupling of the push-pull and $PC_{61}BM$-derived units within the dyad as **TPA-T-C$_{60}$** exhibits almost the same TA spectra and dynamics in the first few hundred picoseconds as the **TPA-T-MCA** reference push-pull compound alone. Thus, we attribute the spectral features of **TPA-T-C$_{60}$** to singlet excitons of the push-pull block. Excitons are spectrally characterized by a positive change in transmission assigned to ground state photo-bleaching (PB), initially seen between 2.3 and 3 eV (413 – 540 nm), corresponding well to the UV-vis ground state absorption spectrum of **TPA-T-MCA**. Two more positive peaks between 1.57 and 2.07 eV are assigned to stimulated emission (SE), as they overlap with the lower energy tail of the PL spectra of solutions and exhibit the same kinetics as the PL (see Figure S16). Finally, two photoinduced absorption (PA) peaks (negative features) initially centered around 1.78 eV and 2.18 eV, blue-shift during the first 50 ps, likely due to solvent relaxation, to 2.25 eV for the highest energy peak, while the lower energy peak disappears, as it shifts to 1.9 eV, where it is superimposed by the (positive) stimulated emission. After solvent relaxation, the signal in **TPA-T-MCA** decays without any further spectral evolution on the ns timescale as excitons recombine. This decay is faster in **TPA-T-C$_{60}$**, in good agreement with the t-PL (see Figure S16) and PL-quenching experiments.

In **TPA-T-C$_{60}$** only, an additional feature appears in the nanosecond timescale: a very broad photoinduced absorption, peaking around 1.7 eV and strongly resembling the signature of triplet states in $PC_{61}BM$ solutions (see Figure S17 and Ref [85]). This spectral signature is thus attributed to triplet excitons localized on the $PC_{61}BM$-derived building block of the dyad. Thus, this result shows that the emission quenching of the push-pull moiety of **TPA-T-C$_{60}$** in solution, as observed previously by steady-state emission experiments, is related to energy transfer to the $PC_{61}BM$-derived building block.

The lack of electronic coupling between the push-pull and $PC_{61}BM$-derived blocks of the dyad seen in solution is very different from the situation in thin films. The TA spectra of films of neat **TPA-T-MCA** are very similar to those observed in solution (see dashed line in Figure 7c), with only the SE contribution missing due to the enhanced non-radiative character of electronic transitions in aggregates. However, the TA spectra of **TPA-T-C$_{60}$** films exhibit very different shape and kinetics (see Figure 7c). **TPA-T-C$_{60}$** spectra have the same ground state bleach as the neat building block (broad peak between 2.4 and 3.3 eV), but the region of photo-induced

absorption is dominated by two photo-induced absorption bands (from 1 to 1.45 eV and 1.8 to 2.4 eV), separated by a plateau. The whole photoinduced absorption is initially present and exhibits almost no spectral evolution up to the microsecond time scale (*vide infra*). It is very similar to the feature dominating the spectra of blends of **TPA-T-MCA** and **$PC_{61}BM$** (Figure S18). The positions of the peaks are the same as those observed upon oxidation of the dyad in solution by spectroelectrochemistry (see Figure 3 and Figure S18). However, the peaks are broader, likely due to solution narrowing observed in the spectroelectrochemistry experiments. We thus attribute the peaks to charge carriers generated ultrafast.

Interestingly, while almost no spectral evolution is seen, the magnitude of the charge carrier signal increases up to one nanosecond (see also in Figure S18), which indicates diffusion-limited exciton dissociation. Spectrally, this is only associated to a slight decrease of the relative weight of the low-energy PA peak, which indicates that the generated charges originate from an excited state with small absorption cross section, as usually is the case for **$PC_{61}BM$** excited states (see for example on Figure 3 the very low signal from the anions in the **$PC_{61}BM$**-derived block compared to the cations in the **TPA-T** block, in spite of almost identical reduction and oxidation currents). To confirm this hypothesis, we reconstructed the PA part of the TA spectra that evolves in time by a sum of contributions from: i) charge carriers, ii) singlet excitons derived from **$PC_{61}BM$** solution spectra, and iii) the triplets excitons determined from the **$PC_{61}BM$**-derived block of **TPA-T-$C_{60}$** in solution (to account for the slower decay of the plateau-like feature). Multivariate curve resolution analysis (MCR)[86,87] was employed to extract the component dynamics and spectra. Reference spectra for charges and triplets in the **$PC_{61}BM$**-derived block (from **TPA-T-$C_{60}$** solutions at ns time scale) were used for the MCR analysis and the absorption spectrum of singlet excitons of **$PC_{61}BM$** was allowed to vary around an initial guess corresponding to the spectrum of singlet excitons of **$PC_{61}BM$** solutions. The precise details of the determination/extraction of the reference spectra can be found in the S.I. As shown in Figure 8a, we obtained an excellent match between the experimental and reconstructed spectral data by using the three contributions determined by MCR. The component kinetics (Figure 8c) confirm that the slow component of the rise of the charge-induced PA is associated with the quenching of the $PC_{61}BM$-block exciton signal, while the recombination of charges appears to lead to the formation of triplets in the $PC_{61}BM$-derived block. The presence of relatively long-lived excitons is rather unexpected in small molecule single component solar cells. It appears that the C6-spacer

acts as an efficient insulator between the donor and acceptor blocks, forcing charge transfer to occur exclusively inter-molecularly at least in a non-negligible fraction of the film. Besides, this confirms the existence of $PC_{61}BM$-rich regions in **TPA-T-C$_{60}$** as suspected from the TEM images in line with the large electron mobility observed by SCLC.

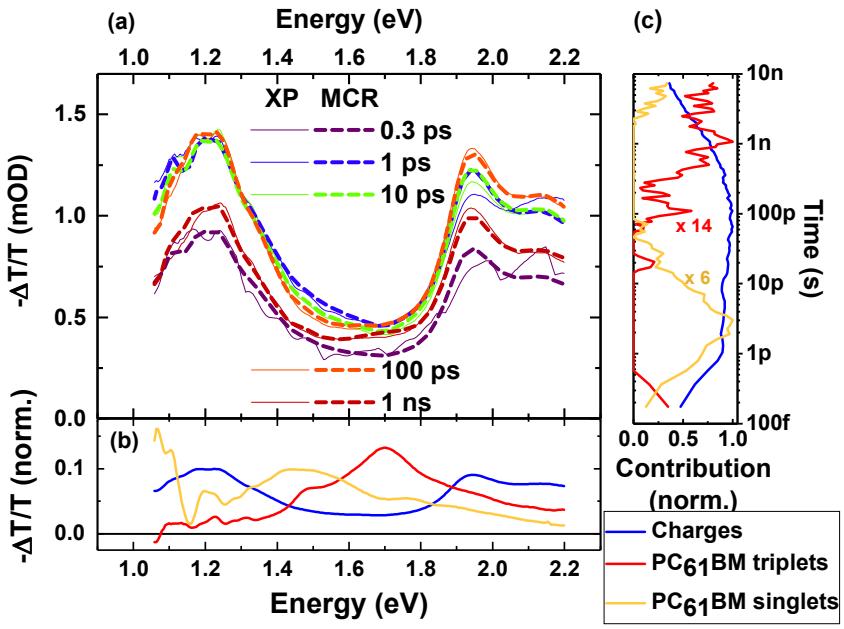


**Figure 8.** Multivariate curve resolution analysis of the photoinduced absorption region of the sub-ns TA spectra for an excitation fluence of 15 $\mu$ J/cm$^2$ (excitation wavelength 480 nm). (a) Comparison of the experimental data to the reconstructed data. Normalized spectral shape (b) and time dependent magnitude (c) of the TA signal originating from each component.

In order to evaluate further the efficiency of this charge generation channel, the proportionality factor, namely the absorption cross section of charges, needs to be known to extract the density of charge carriers from their optical response. This was achieved by comparing the optical signal (from TA) at 10 ns to the quantity of charges extracted from a device in a Time-Delayed Collection Field (TDCF) experiment after the same delay of 10 ns, as recently presented by us for other BHJ systems.[83] Both experiments (TA and TDCF) used the same laser source, and the density of absorbed photons in the device stack was determined by the transfer matrix formalism (see Figure S15). More details can be found in the SI. With the charge carrier absorption cross section in hand (Figure 9b), the density of charges was calculated at each time delay. Here we see that for the lowest fluence measured (which corresponds to an

illumination intensity still far above 1 sun), the density of charges initially generated equals the density of absorbed photons (within the error bars).

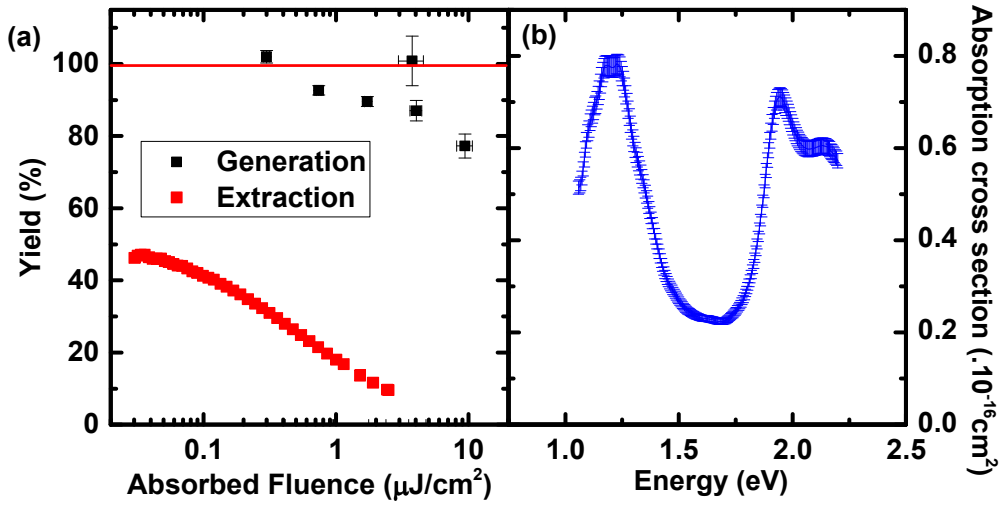


**Figure 9.** (a) Evolution of the TDCF charge extraction yield with fluence (number of extracted charges per absorbed photon) obtained upon excitation at on a device biased at $V_{OC}$ with a 800 ps 532 nm laser pulse followed by extraction from 10 ns until 1 μs by a 1.5 V reverse bias pulse), and charge generation yield (number of charges generated per absorbed photons) determined from the amplitude of the charge-induced absorption signal (from MCR analysis) using the absorption cross section of charges to recalculate the TA signal into a density of charges. (b) Absorption cross section obtained by comparing the TA signal at 10 ns to the number of charges extracted after the same delay time and under the same excitation conditions in a TDCF experiment (details in the S.I.).

**2.5.3. Charge carrier recombination.** As we can see from Figure 9, while the charge generation efficiency approaches unity, only a small fraction can eventually be extracted from the device, even if extraction is facilitated by a collection field as in the TDCF experiment. To understand the origin of the losses, we turned to transient absorption measurements in the time range relevant for charge extraction (ns to hundreds of μs). Similar to the sub-ps to ns experiments, multivariate curve resolution was used and enabled us to extract the contribution of charges to the total photoinduced absorption (alongside the contribution of triplets, see details in S.I.). The normalized dynamics are presented in Figure 10. The fluence dependent dynamics were fitted by a two-pool recombination model, as previously applied to TA data of other BHJ systems.[83, 88] Briefly, this model assumes that charges are distributed between two pools after charge transfer: a fraction $f$ of the charges separates entirely and overcomes the coulombic attraction and successively recombines non-geminately with an apparent recombination order $\lambda+1$, empirically found to be higher than 2, and a prefactor $k_\lambda$. On the other hand, the fraction $1-f$

accounts for charge pairs that have not escaped their counter-charge and remain trapped at the interface where they recombine geminately. This pool exhibits an exponential decay associated to a lifetime $\tau$ independent of the excitation fluence.

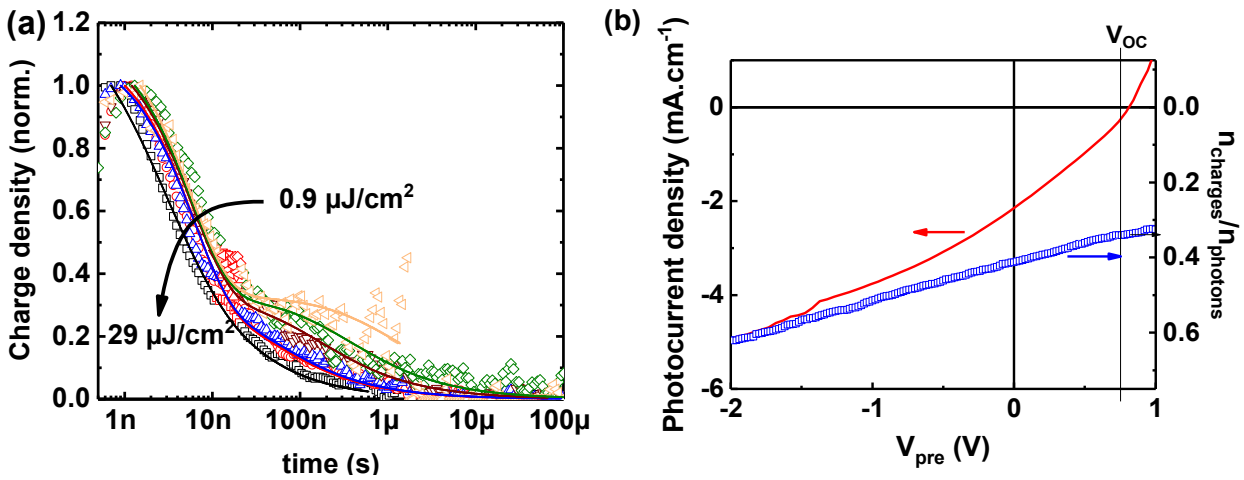


**Figure 10.** (a) Fluence dependence of ns-µs charge carrier dynamics and fit of the charge recombination dynamics to two-pool model. (b) Efficiency of the collection of charges (symbols, right axis) by the application of a collection voltage of -3 V 10 ns after the photoexcitation by a 532 nm pulse of intensity 1 µJ/cm$^2$ as function of the bias voltage ($V_{pre}$) applied during the pulse (reported to the density of absorbed photons calculated by transfer matrix simulation of the device) compared with the photocurrent (continuous line, left axis).

**Table 3.** Recombination parameters extracted from a global fit of the fluence-dependent charge-induced absorption decay to a two-pool model, equivalent bimolecular recombination coefficient $k_2$ extrapolated from $\lambda$ and $k_\lambda$ for a charge density of $5\times10^{15}$ cm$^{-3}$ and comparison with the theoretical Langevin recombination coefficient $k_{langevin} = q(\mu_e + \mu_h)/\varepsilon$, where $\mu_e$ and $\mu_h$ were obtained by SCLC (*vide supra*), $\varepsilon = \varepsilon_0\,\varepsilon_r$, the dielectric constant, where $\varepsilon_r$ is estimated by ellipsometry measurements (see S.I.).

| $f$ | $\tau$ [ns] | $\lambda + 1$ | $k_\lambda$ [cm$^{3(\lambda-1)}$s$^{-1}$] | $k_2$ [cm$^3$s$^{-1}$] | $k_{langevin}$ [cm$^3$s$^{-1}$] | $k_2/k_{langevin}$ |
|---|---|---|---|---|---|---|
| 0.33 ± 0.01 | 5.8 ± 0.1 | 2.52 ± 0.01 | 6.7 ± 3.5 ×10$^{-20}$ | 1 ± 0.5×10$^{-11}$ | 2.6×10$^{-10}$ | 0.04 |

Table 3 presents the parameters extracted from the fit of the TA data to the two-pool model. As can be seen also from Figure 10a, as much as 66% of the charges recombine geminately (*1-f*), following a fluence-independent decay. This is supported by Time Delayed Collection Field experiments (Figure 10b): when the device is measured in open circuit conditions ($V_{pre} = V_{OC}$), the number of extracted charges corresponds to 33% of the total number of absorbed photons. However, this pronounced geminate recombination is alleviated, when an

electric field is applied. This is clearly seen from the increase of the number of extracted charges when applying a zero or negative bias during the photoexcitation pulse ($V_{pre} \leq 0V$).

Turning to non-geminate recombination, the rate extracted from the two-pool model was recalculated for a typical charge density in a working device to compare it with previously reported systems. An equivalent bimolecular recombination prefactor $k_2$ (calculation in the S.I.) of $k_2 = 1\times10^{-11}$ cm$^3$/s for a charge density of $5\times10^{15}$ cm$^{-3}$ was determined. Thus, **TPA-T-C$_{60}$** exhibits a recombination rate at the higher end of the range typically found for organic semiconductors.[89] This rather high recombination rate combined with a relatively low hole mobility and large difference between hole and electron mobilities[90] results in an unfavorable competition between charge extraction and recombination as can be seen in Figure 10b. Here, the bias dependence of the photocurrent is much stronger than can be explained by field-dependent charge generation alone: in fact, for low internal fields (voltage close to $V_{OC}$) the longer extraction time results in increased recombination losses.

## 3. Conclusions

A donor-σ-acceptor molecular dyad, consisting of a triphenylamine-thiophene-based push-pull π-conjugated system linked to a $C_{60}$ unit through a non-conjugated σ linker, was synthesized in good yields and used as photoactive material in single-component organic solar cells. A power conversion efficiency of only 0.4% was obtained, mostly due to the modest fill-factor *FF* of 29%, originating in part from unbalanced hole- and electron-mobilities. Spectroscopic analysis using transient absorption and time-delayed collection field experiments showed quantitative photon-to-charge conversion, by ultrafast and diffusion-limited dissociation of excitons. However, charge separation was found to be strongly field dependent, significantly limiting the fill factor, which is even further reduced by a strong competition of recombination of separated charges with charge extraction. TA also showed relatively long-lived fullerene excitons, suggesting the existence of rather pure domains of the $PC_{61}BM$ derived block however, too small to be detected by morphological studies. The high electron mobility further indicates that those domains are probably percolated.

These results are very encouraging, as they reveal that charge percolation is possible in these devices. While the devices could already be applied as photosensors, since efficient photocurrent generation is achieved at negative bias, we expect that achieving also donor domains percolation would further balance the mobilities and thereby reduce the field dependence of current extraction and probably also charge separation. Overall, our results demonstrate that single-component organic solar cells can be prepared with an easily accessible push-pull-σ-$C_{60}$ dyad. The concept can be easily extended to other building blocks with novel electrochemical and optical properties thanks to the adaptable synthetic methodology. Finally, the photophysics of the single-component organic solar cells strongly suggest that it is crucial to design new molecular dyads which exhibit enhanced self-assembly properties for optimized nanophase separation.

**Supporting Information**

Synthesis; $^{1}$H NMR and $^{13}$C NMR spectra; MALDI-TOF and high resolution mass spectra; UV−vis absorption spectra; fabrication and characterization of devices; ellipsometry and transfer matrix simulation; transient absorption and time resolved photoluminescence measurements; multivariate curve resolution; time delayed collection field; two-pool model

**Acknowledgments**

The RFI LUMOMAT from the Région Pays de la Loire is acknowledged for the PhD grant of A. Labrunie. We thank also the PIAM (*Plateforme d'Ingénierie et Analyses Moléculaires*) of the University of Angers for the characterization of organic compounds and R. Mallet, from the SCIAM of the University of Angers for TEM experiments. Jonhson Mattey is acknowledged for the gift of $PdCl_2$ used for the preparation of $Pd(PPh_3)_4$ catalyst. The research reported in this publication was supported by funding from King Abdullah University of Science and Technology (KAUST). M. Wohlfahrt acknowledges a VSRP internship from KAUST.

**References**

1. Yu, G.; Gao, J.; Hummelen, J. C.; Wudl, F.; Heeger, A. J. Polymer Photovoltaic Cells: Enhanced Efficiencies via a Network of Internal Donor-Acceptor Heterojunctions. *Science* **1995,** *270*, 1789-1791.
2. Shaheen, S. E.; Brabec, C. J.; Sariciftci, N. S.; Padinger, F.; Fromherz, T.; Hummelen, J. C. 2.5% efficient organic plastic solar cells. *Appl. Phys. Lett.* **2001,** *78*, 841-843.
3. Gunes, S.; Neugebauer, H.; Sariciftci, N. S. Conjugated polymer-based organic solar cells. *Chem. Rev.* **2007,** *107*, 1324-1338.
4. Thompson, B. C.; Frechet, J. M. Polymer-fullerene composite solar cells. *Angew. Chem. Int. Ed.* **2008,** *47*, 58-77.
5. Gendron, D.; Leclerc, M. New conjugated polymers for plastic solar cells. *Energy Environ. Sci.* **2011,** *4*, 1225-1237.
6. Li, Y. Molecular Design of Photovoltaic Materials for Polymer Solar Cells: Toward Suitable Electronic Energy Levels and Broad Absorption. *Acc. Chem. Res.* **2012,** *45*, 723-733.
7. Dou, L.; Liu, Y.; Hong, Z.; Li, G.; Yang, Y. Low-Bandgap Near-IR Conjugated Polymers/Molecules for Organic Electronics. *Chem. Rev.* **2015,** *115*, 12633-12665.
8. Lu, L.; Zheng, T.; Wu, Q.; Schneider, A. M.; Zhao, D.; Yu, L. Recent Advances in Bulk Heterojunction Polymer Solar Cells. *Chem. Rev.* **2015,** *115*, 12666-12731.
9. Liu, C.; Wang, K.; Gong, X.; Heeger, A. J. Low bandgap semiconducting polymers for polymeric photovoltaics. *Chem. Soc. Rev.* **2016,** *45*, 4825-4846.
10. Roncali, J. Molecular Bulk Heterojunctions: An Emerging Approach to Organic Solar Cells. *Acc. Chem. Res.* **2009,** *42*, 1719-1730.
11. Mishra, A.; Bauerle, P. Small molecule organic semiconductors on the move: promises for future solar energy technology. *Angew. Chem. Int. Ed.* **2012,** *51*, 2020-2067.
12. Li, M.; Ni, W.; Wan, X.; Zhang, Q.; Kan, B.; Chen, Y. Benzo[1,2-b:4,5-b']dithiophene (BDT)-based small molecules for solution processed organic solar cells. *J. Mater. Chem. A* **2015,** *3*, 4765-4776.
13. Malytskyi, V.; Simon, J.-J.; Patrone, L.; Raimundo, J.-M. Thiophene-based push–pull chromophores for small molecule organic solar cells (SMOSCs). *RSC Adv.* **2015,** *5*, 354-397.
14. Liu, Y.; Zhao, J.; Li, Z.; Mu, C.; Ma, W.; Hu, H.; Jiang, K.; Lin, H.; Ade, H.; Yan, H. Aggregation and morphology control enables multiple cases of high-efficiency polymer solar cells. *Nat. Commun.* **2014,** *5*, 5293.
15. Zhao, J.; Li, Y.; Yang, G.; Jiang, K.; Lin, H.; Ade, H.; Ma, W.; Yan, H. Efficient organic solar cells processed from hydrocarbon solvents. *Nat. Energy* **2016,** *1*, 15027.
16. Park, K. H.; An, Y.; Jung, S.; Park, H.; Yang, C. The use of an n-type macromolecular additive as a simple yet effective tool for improving and stabilizing the performance of organic solar cells. *Energy Environ. Sci.* **2016,** *9*, 3464-3471.
17. Xiao, S.; Zhang, Q.; You, W. Molecular Engineering of Conjugated Polymers for Solar Cells: An Updated Report. *Adv. Mater.* **2017,** *29*, 1601391.
18. Kan, B.; Li, M.; Zhang, Q.; Liu, F.; Wan, X.; Wang, Y.; Ni, W.; Long, G.; Yang, X.; Feng, H.; Zuo, Y.; Zhang, M.; Huang, F.; Cao, Y.; Russell, T. P.; Chen, Y. A series of simple oligomer-like small molecules

based on oligothiophenes for solution-processed solar cells with high efficiency. *J. Am. Chem. Soc.* **2015,** *137*, 3886-3893.
19. Lin, Y.; Zhan, X. Non-fullerene acceptors for organic photovoltaics: an emerging horizon. *Mater. Horiz.* **2014,** *1*, 470-488.
20. Nielsen, C. B.; Holliday, S.; Chen, H. Y.; Cryer, S. J.; McCulloch, I. Non-fullerene electron acceptors for use in organic solar cells. *Acc. Chem. Res.* **2015,** *48*, 2803-2812.
21. McAfee, S. M.; Topple, J. M.; Hill, I. G.; Welch, G. C. Key components to the recent performance increases of solution processed non-fullerene small molecule acceptors. *J. Mater. Chem. A* **2015,** *3*, 16393-16408.
22. Zhan, C.; Zhang, X.; Yao, J. New advances in non-fullerene acceptor based organic solar cells. *RSC Adv.* **2015,** *5*, 93002-93026.
23. Zhan, C.; Yao, J. More than Conformational "Twisting" or "Coplanarity": Molecular Strategies for Designing High-Efficiency Nonfullerene Organic Solar Cells. *Chem. Mater.* **2016,** *28*, 1948-1964.
24. Li, S.; Zhang, Z.; Shi, M.; Li, C. Z.; Chen, H. Molecular electron acceptors for efficient fullerene-free organic solar cells. *Phys. Chem. Chem. Phys.* **2017,** *19*, 3440-3458.
25. Chen, W.; Zhang, Q. Recent progress in non-fullerene small molecule acceptors in organic solar cells (OSCs). *J. Mater. Chem. C* **2017,** *5*, 1275-1302.
26. Zhao, W.; Li, S.; Yao, H.; Zhang, S.; Zhang, Y.; Yang, B.; Hou, J. Molecular Optimization Enables over 13% Efficiency in Organic Solar Cells. *J. Am. Chem. Soc.* **2017,** *139*, 7148-7151.
27. Peumans, P.; Yakimov, A.; Forrest, S. R. Small molecular weight organic thin-film photodetectors and solar cells. *J. Appl. Phys.* **2003,** *93*, 3693-3723.
28. Schlenker, C. W.; Thompson, M. E. The molecular nature of photovoltage losses in organic solar cells. *Chem. Commun.* **2011,** *47*, 3702-3716.
29. Janssen, R. A. J.; Nelson, J. Factors Limiting Device Efficiency in Organic Photovoltaics. *Adv. Mater.* **2013,** *25*, 1847-1858.
30. Huang, Y.; Kramer, E. J.; Heeger, A. J.; Bazan, G. C. Bulk heterojunction solar cells: morphology and performance relationships. *Chem. Rev.* **2014,** *114*, 7006-7043.
31. Dang, M. T.; Hirsch, L.; Wantz, G.; Wuest, J. D. Controlling the Morphology and Performance of Bulk Heterojunctions in Solar Cells. Lessons Learned from the Benchmark Poly(3-hexylthiophene):[6,6]-Phenyl-C61-butyric Acid Methyl Ester System. *Chem. Rev.* **2013,** *113*, 3734-3765.
32. Nierengarten, J.-F.; Eckert, J.-F.; Nicoud, J.-F.; Ouali, L.; Krasnikov, V.; Hadziioannou, G. Synthesis of a C60-oligophenylenevinylene hybrid and its incorporation in a photovoltaic device. *Chem. Commun.* **1999,** 617-618.
33. Cravino, A.; Sariciftci, N. S. Double-cable polymers for fullerene based organic optoelectronic applications. *J. Mater. Chem.* **2002,** *12*, 1931-1943.
34. Segura, J. L.; Martin, N.; Guldi, D. M. Materials for organic solar cells: the C60/pi-conjugated oligomer approach. *Chem. Soc. Rev.* **2005,** *34*, 31-47.
35. Roncali, J. Linear π-conjugated systems derivatized with C60-fullerene as molecular heterojunctions for organic photovoltaics. *Chem. Soc. Rev.* **2005,** *34*, 483-495.
36. Roncali, J. Single Material Solar Cells: the Next Frontier for Organic Photovoltaics? *Adv. Energy Mater.* **2011,** *1*, 147-160.
37. Wang, M.; Wudl, F. Top-down meets bottom-up: organized donor–acceptor heterojunctions for organic solar cells. *J. Mater. Chem.* **2012,** *22*, 24297-24314.
38. Figueira-Duarte, T. M.; Gegout, A.; Nierengarten, J. F. Molecular and supramolecular C60-oligophenylenevinylene conjugates. *Chem. Commun.* **2007,** 109-119.
39. van Hal, P. A.; Beckers, E. H.; Meskers, S. C.; Janssen, R. A.; Jousselme, B.; Blanchard, P.; Roncali, J. Orientational effect on the photophysical properties of quaterthiophene-C60 dyads. *Chem. Eur. J.* **2002,** *8*, 5415-5429.

40. van Hal, P. A.; Meskers, S. C. J.; Janssen, R. A. J. Photoinduced energy and electron transfer in oligo(p-phenylene vinylene)-fullerene dyads. *Appl. Phys. A* **2004,** *79*, 41-46.
41. Kirner, S.; Sekita, M.; Guldi, D. M. 25th anniversary article: 25 years of fullerene research in electron transfer chemistry. *Adv. Mater.* **2014,** *26*, 1482-93.
42. Neuteboom, E. E.; Meskers, S. C.; van Hal, P. A.; van Duren, J. K.; Meijer, E. W.; Janssen, R. A.; Dupin, H.; Pourtois, G.; Cornil, J.; Lazzaroni, R.; Bredas, J. L.; Beljonne, D. Alternating oligo(p-phenylene vinylene)--perylene bisimide copolymers: synthesis, photophysics, and photovoltaic properties of a new class of donor--acceptor materials. *J. Am. Chem. Soc.* **2003,** *125*, 8625-8638.
43. Wang, M.; Heeger, A. J.; Wudl, F. Self-assembly of a fullerene poly(3-hexylthiophene) dyad. *Small* **2011,** *7*, 298-301.
44. Guldi, D. M.; Luo, C.; Swartz, A.; Gómez, R.; Segura, J. L.; Martín, N.; Brabec, C.; Sariciftci, N. S. Molecular Engineering of C60-Based Conjugated Oligomer Ensembles: Modulating the Competition between Photoinduced Energy and Electron Transfer Processes. *J. Org. Chem.* **2002,** *67*, 1141-1152.
45. Antonietta Loi, M.; Denk, P.; Hoppe, H.; Neugebauer, H.; Winder, C.; Meissner, D.; Brabec, C.; Serdar Sariciftci, N.; Gouloumis, A.; Vázquez, P.; Torres, T. Long-lived photoinduced charge separation for solar cell applications in phthalocyanine–fulleropyrrolidine dyad thin films. *J. Mater. Chem.* **2003,** *13*, 700-704.
46. Fernández, G.; Sánchez, L.; Veldman, D.; Wienk, M. M.; Atienza, C.; Guldi, D. M.; Janssen, R. A. J.; Martín, N. Tetrafullerene Conjugates for All-Organic Photovoltaics. *J. Org. Chem.* **2008,** *73*, 3189-3196.
47. Eckert, J.-F.; Nicoud, J.-F.; Nierengarten, J.-F.; Liu, S.-G.; Echegoyen, L.; Barigelletti, F.; Armaroli, N.; Ouali, L.; Krasnikov, V.; Hadziioannou, G. Fullerene−Oligophenylenevinylene Hybrids: Synthesis, Electronic Properties, and Incorporation in Photovoltaic Devices. *J. Am. Chem. Soc.* **2000,** *122*, 7467-7479.
48. Peeters, E.; van Hal, P. A.; Knol, J.; Brabec, C. J.; Sariciftci, N. S.; Hummelen, J. C.; Janssen, R. A. J. Synthesis, Photophysical Properties, and Photovoltaic Devices of Oligo(p-phenylene vinylene)-fullerene Dyads. *J. Phys. Chem. B* **2000,** *104*, 10174-10190.
49. Lindner, S. M.; Huttner, S.; Chiche, A.; Thelakkat, M.; Krausch, G. Charge separation at self-assembled nanostructured bulk interface in block copolymers. *Angew. Chem. Int. Ed.* **2006,** *45*, 3364-3368.
50. Sommer, M.; Huettner, S.; Thelakkat, M., Donor–acceptor block copolymers for photovoltaic applications. *J. Mater. Chem.* **2010,** *20*, 10788-10797.
51. Miyanishi, S.; Zhang, Y.; Tajima, K.; Hashimoto, K. Fullerene attached all-semiconducting diblock copolymers for stable single-component polymer solar cells. *Chem. Commun.* **2010,** *46*, 6723-6725.
52. Pierini, F.; Lanzi, M.; Nakielski, P.; Pawłowska, S.; Urbanek, O.; Zembrzycki, K.; Kowalewski, T. A. Single-Material Organic Solar Cells Based on Electrospun Fullerene-Grafted Polythiophene Nanofibers. *Macromolecules* **2017,** *50*, 4972-4981.
53. Feng, G.; Li, J.; Colberts, F. J. M.; Li, M.; Zhang, J.; Yang, F.; Jin, Y.; Zhang, F.; Janssen, R. A. J.; Li, C.; Li, W. "Double-Cable" Conjugated Polymers with Linear Backbone toward High Quantum Efficiencies in Single-Component Polymer Solar Cells. *J. Am. Chem. Soc.* **2017,** *139*, 18647-18656.
54. Bu, L.; Guo, X.; Yu, B.; Qu, Y.; Xie, Z.; Yan, D.; Geng, Y.; Wang, F. Monodisperse co-oligomer approach toward nanostructured films with alternating donor-acceptor lamellae. *J. Am. Chem. Soc.* **2009,** *131*, 13242-13243.
55. Qu, J.; Gao, B.; Tian, H.; Zhang, X.; Wang, Y.; Xie, Z.; Wang, H.; Geng, Y.; Wang, F. Donor–spacer–acceptor monodisperse conjugated co-oligomers for efficient single-molecule photovoltaic cells based on non-fullerene acceptors. *J. Mater. Chem. A* **2014,** *2*, 3632-3640.
56. Schwartz, P. O.; Biniek, L.; Zaborova, E.; Heinrich, B.; Brinkmann, M.; Leclerc, N.; Mery, S. Perylenediimide-based donor-acceptor dyads and triads: impact of molecular architecture on self-assembling properties. *J. Am. Chem. Soc.* **2014,** *136*, 5981-5992.

57. Biniek, L.; Schwartz, P.-O.; Zaborova, E.; Heinrich, B.; Leclerc, N.; Méry, S.; Brinkmann, M. Zipper-like molecular packing of donor–acceptor conjugated co-oligomers based on perylenediimide. *J. Mater. Chem. C* **2015,** *3*, 3342-3349.
58. Roncali, J.; Leriche, P.; Blanchard, P. Molecular materials for organic photovoltaics: small is beautiful. *Adv. Mater.* **2014,** *26*, 3821-3838.
59. Nishizawa, T.; Lim, H. K.; Tajima, K.; Hashimoto, K. Efficient dyad-based organic solar cells with a highly crystalline donor group. *Chem. Commun.* **2009,** 2469-2471.
60. Izawa, S.; Hashimoto, K.; Tajima, K. Morphological stability of organic solar cells based upon an oligo(p-phenylenevinylene)-C70 dyad. *Phys. Chem. Chem. Phys.* **2012,** *14*, 16138-16142.
61. Izawa, S.; Hashimoto, K.; Tajima, K. Efficient charge generation and collection in organic solar cells based on low band gap dyad molecules. *Chem. Commun.* **2011,** *47*, 6365-6367.
62. Chen, T. L.; Zhang, Y.; Smith, P.; Tamayo, A.; Liu, Y.; Ma, B. Diketopyrrolopyrrole-containing oligothiophene-fullerene triads and their use in organic solar cells. *ACS Appl. Mater. Interfaces* **2011,** *3*, 2275-2280.
63. Cao, J.; Du, X.; Chen, S.; Xiao, Z.; Ding, L. A dumbbell-like A-D-A molecule for single-component organic solar cells. *Phys. Chem. Chem. Phys.* **2014,** *16*, 3512-3514.
64. Narayanaswamy, K.; Venkateswararao, A.; Nagarjuna, P.; Bishnoi, S.; Gupta, V.; Chand, S.; Singh, S. P. An Organic Dyad Composed of Diathiafulvalene-Functionalized Diketopyrrolopyrrole-Fullerene for Single-Component High-Efficiency Organic Solar Cells. *Angew. Chem. Int. Ed.* **2016,** *55*, 12334-12337.
65. Nguyen, T. L.; Lee, T. H.; Gautam, B.; Park, S. Y.; Gundogdu, K.; Kim, J. Y.; Woo, H. Y. Single Component Organic Solar Cells Based on Oligothiophene-Fullerene Conjugate. *Adv. Funct. Mater.* **2017,** *27*, 1702474.
66. Leliège, A.; Le Régent, C. H.; Allain, M.; Blanchard, P.; Roncali, J. Structural modulation of internal charge transfer in small molecular donors for organic solar cells. *Chem. Commun.* **2012,** *48*, 8907-8909.
67. Choi, J. W.; Kim, C.-H.; Pison, J.; Oyedele, A.; Tondelier, D.; Leliège, A.; Kirchner, E.; Blanchard, P.; Roncali, J.; Geffroy, B. Exploiting the potential of 2-((5-(4-(diphenylamino)phenyl)thiophen-2-yl)methylene)malononitrile as an efficient donor molecule in vacuum-processed bulk-heterojunction organic solar cells. *RSC Adv.* **2014,** *4*, 5236-5242.
68. Labrunie, A.; Jiang, Y.; Baert, F.; Leliège, A.; Roncali, J.; Cabanetos, C.; Blanchard, P. Small molecular push–pull donors for organic photovoltaics: effect of the heterocyclic π-spacer. *RSC Adv.* **2015,** *5*, 102550-102554.
69. Leliège, A.; Grolleau, J.; Allain, M.; Blanchard, P.; Demeter, D.; Rousseau, T.; Roncali, J. Small D-pi-A systems with o-phenylene-bridged accepting units as active materials for organic photovoltaics. *Chem. Eur. J.* **2013,** *19*, 9948-9960.
70. Jiang, Y.; Cabanetos, C.; Allain, M.; Liu, P.; Roncali, J. Manipulation of the band gap and efficiency of a minimalist push–pull molecular donor for organic solar cells. *J. Mater. Chem. C* **2015,** *3*, 5145-5151.
71. Mohamed, S.; Demeter, D.; Laffitte, J. A.; Blanchard, P.; Roncali, J. Structure-properties relationships in triarylamine-based donor-acceptor molecules containing naphtyl groups as donor material for organic solar cells. *Sci. Rep.* **2015,** *5*, 9031.
72. Baert, F.; Cabanetos, C.; Allain, M.; Silvestre, V.; Leriche, P.; Blanchard, P. Thieno[2,3-b]indole-Based Small Push-Pull Chromophores: Synthesis, Structure, and Electronic Properties. *Org. Lett.* **2016,** *18*, 1582-1585.
73. Sissa, C.; Parthasarathy, V.; Drouin-Kucma, D.; Werts, M. H.; Blanchard-Desce, M.; Terenziani, F. The effectiveness of essential-state models in the description of optical properties of branched push-pull chromophores. *Phys. Chem. Chem. Phys.* **2010,** *12*, 11715-11727.
74. Grolleau, J.; Gohier, F.; Allain, M.; Legoupy, S.; Cabanetos, C.; Frère, P. Rapid and green synthesis of complementary D-A small molecules for organic photovoltaics. *Org. Electron.* **2017,** *42*, 322-328.

75. Miyanishi, S.; Zhang, Y.; Hashimoto, K.; Tajima, K. Controlled Synthesis of Fullerene-Attached Poly(3-alkylthiophene)-Based Copolymers for Rational Morphological Design in Polymer Photovoltaic Devices. *Macromolecules* **2012,** *45*, 6424-6437.
76. Hummelen, J. C.; Knight, B. W.; LePeq, F.; Wudl, F.; Yao, J.; Wilkins, C. L. Preparation and Characterization of Fulleroid and Methanofullerene Derivatives. *J. Org. Chem.* **1995,** *60*, 532-538.
77. Diacon, A.; Derue, L.; Lecourtier, C.; Dautel, O.; Wantz, G.; Hudhomme, P. Cross-linkable azido C60-fullerene derivatives for efficient thermal stabilization of polymer bulk-heterojunction solar cells. *J. Mater. Chem. C* **2014,** *2*, 7163-7167.
78. Brouwer, A. M. Standards for photoluminescence quantum yield measurements in solution. *Pure Appl. Chem.* **2011,** *83*, 2213-2228.
79. Bures, F. Fundamental aspects of property tuning in push-pull molecules. *RSC Adv.* **2014,** *4*, 58826-58851.
80. Jiang, Y.; Gindre, D.; Allain, M.; Liu, P.; Cabanetos, C.; Roncali, J. A Mechanofluorochromic Push–Pull Small Molecule with Aggregation-Controlled Linear and Nonlinear Optical Properties. *Adv. Mater.* **2015,** *27*, 4285-4289.
81. Guldi, D. M.; Prato, M. Excited-State Properties of C60Fullerene Derivatives. *Acc. Chem. Res.* **2000,** *33*, 695-703.
82. Marcos Ramos, A.; Rispens, M. T.; Hummelen, J. C.; Janssen, R. A. J. A poly(p-phenylene ethynylene vinylene) with pendant fullerenes. *Synth. Met.* **2001,** *119*, 171-172.
83. Gorenflot, J.; Paulke, A.; Piersimoni, F.; Wolf, J.; Kan, Z.; Cruciani, F.; Labban, A. E.; Neher, D.; Beaujuge, P. M.; Laquai, F. From Recombination Dynamics to Device Performance: Quantifying the Efficiency of Exciton Dissociation, Charge Separation, and Extraction in Bulk Heterojunction Solar Cells with Fluorine-Substituted Polymer Donors. *Adv. Energy Mater.* **2018,** *8*, 1701678.
84. Pettersson, L. A. A.; Roman, L. S.; Inganäs, O. Modeling photocurrent action spectra of photovoltaic devices based on organic thin films. *J. Appl. Phys.* **1999,** *86*, 487-496.
85. Chow, P. C.; Albert-Seifried, S.; Gelinas, S.; Friend, R. H. Nanosecond intersystem crossing times in fullerene acceptors: implications for organic photovoltaic diodes. *Adv. Mater.* **2014,** *26*, 4851-4854.
86. Jaumot, J.; Gargallo, R.; de Juan, A.; Tauler, R. A graphical user-friendly interface for MCR-ALS: a new tool for multivariate curve resolution in MATLAB. *Chemom. Intell. Lab. Syst.* **2005,** *76*, 101-110.
87. Howard, I. A. M., H.; Etzold, F.; Gehrig, D.; Laquai F. Transient Absorption Data Analysis by Soft-Modelling. In *Ultrafast Dynamics in Molecules, Nanostructures and Interfaces*, H. G. Gurzadyan, G. L., C. Soci, T. C. Sum, Ed. World Scientific: Singapore, 2014; Vol. 8, pp 53-78.
88. Howard, I. A.; Mauer, R.; Meister, M.; Laquai, F. Effect of morphology on ultrafast free carrier generation in polythiophene:fullerene organic solar cells. *J. Am. Chem. Soc.* **2010,** *132*, 14866-14876.
89. Collins, S. D.; Ran, N. A.; Heiber, M. C.; Nguyen, T.-Q. Small is Powerful: Recent Progress in Solution-Processed Small Molecule Solar Cells. *Adv. Energy Mater.* **2017,** *7*, 1602242.
90. Proctor, C. M.; Love, J. A.; Nguyen, T. Q. Mobility guidelines for high fill factor solution-processed small molecule solar cells. *Adv. Mater.* **2014,** *26*, 5957-5961.

**Table of Contents (TOC) Graphic**